Analyzing the microstructure and mechanical properties of polytetrafluoroethylene fabricated by field-assisted sintering

I. El Aboudi, Ahmed Mdarhri, Olivier Lame, Christian Brosseau, Ali Nourdine, Damien Fabrègue, Guillaume Bonnefont

Analyzing the microstructure and mechanical properties of polytetrafluoroethylene fabricated by field-assisted sintering

I. El Aboudi[1], Ahmed Mdarhri[1], Olivier Lame[2], Christian Brosseau [3,*], Ali Nourdine[4], Damien Fabrègue[5] and Guillaume Bonnefont[2]

[1]Laboratoire de Recherche en Développement Durable & Santé, FSTG Cadi Ayyad University, A. Khattabi, BP 549, 40 000 Marrakech, Morocco

[2]Laboratoire MATEIS, Bât. B. Pascal, Avenue Jean Capelle, 69621 Villeurbanne Cedex France

[3]Univ Brest, CNRS, Lab-STICC, CS, 93837, 6 avenue Le Gorgeu, 29238, Brest Cedex 3, France

[4]Univ. Grenoble Alpes, Univ. Savoie Mont Blanc, CNRS, Grenoble INP, LEPMI, 38000 Grenoble, France

[5]Department of MATEIS-UMR 5510, Avenue Jean Capelle, 69621 Villeurbanne Cedex, France

*Corresponding author

Keywords: PTFE, FAST/SPS process, microstructure, thermal stability, mechanical behavior, modeling

Abstract

The results presented here exploits field-assisted sintering (also known as spark plasma sintering) to elaborate polytetrafluoroethylene (PTFE) dense polymer materials from PTFE powder. This technique is especially suitable for processing viscous polymer materials, e.g. PTFE, which is known to be difficult to melt-process via the usual methods including hot press sintering and hot isostatic pressing. A series of sintered PTFE is prepared at constant sintering temperature and various heating rate and the microstructures formed in this manner are characterized using differential scanning calorimetry, Raman and infrared spectroscopies. Stress-strain curves performed by using both three-point bending and tensile tests highlight a significant dependence of the heating rate on the PTFE microstructure. The stress-strain behavior under large deformations is discussed on the basis of the theory proposed by Haward and Thackray.

I. Introduction

Hyper or partially fluorinated polymers exhibit specific chemical, physical and mechanical properties, e.g. chemical inertness, low surface energy and hydrophobic character, thermal stability, low friction coefficient and low permittivity [1-3]. Recent work shows that polytetrafluoroethylene (PTFE) is an attractive high-performant fluoropolymer for which the market size is estimated to be 70% of the global fluoropolymers market. Reported application examples include insulator materials in electrical cables, load-bearing structural components, nonstick and hydrophobic surfaces, lubrication, biomedical components and fuel-cell systems. PTFE is a high-molecular-weight polymer with specific intermolecular arrangements and conformations which induce complicated phases within crystalline domains [4]. The properties of PTFE origin from the synergy between the high electronegativity of fluorine atom, the strength of carbon-fluorine covalent bond (110 kcal/mole) and the density and nature of intra/intermolecular interactions between the polymer segments [5]. However, PTFE imposes engineering constraints (high melt processing conditions [6]) that prevent use of standard melt-processing methods, i.e. injection, extrusion.

Non-melting processes such as sintering can also serve as the design approach in this context. This method is inspired from powder metallurgy processing techniques. For example, cold compaction followed by sintering at temperature above the melting point of the neat polymer offers a relevant solution. But, this requires a long processing time and is costly, which is also true for other sintering process, e.g. compression molding or isostatic pressing [7]. Recently, one design approach has been explored several authors [8-11]: it consists in applying high velocity impacts at room temperature on a powder filled die to form a green part which is later sintered. By using this technique to elaborate PTFE samples, Poitou and coworkers [11] have successively reduced the processing time (two minutes against several hours) and improved microstructural features, but the mechanical properties of the samples are found to be weak compared to the samples elaborated by conventional sintering methods. In this context, the high velocity compaction method provides a route to process high molecular weight polymers [9, 10], but it requires a long sintering time (more than one hour) and the produced polymer has a brittle mechanical behavior.

The advances outlined in the following directly address the above mentioned limitations via the fast field-assisted sintering technique (FAST), also known as spark plasma sintering, to produce dense PTFE samples conserving their functional, mechanical and physical

properties; a current interest to the polymers science community. Historically, FAST was employed for ceramic and metallic materials products [12]. It is only recently that this technique was adapted to polymers [13]. In short, it consists in applying simultaneously a pressure and an electric current to the sample. The induced Joule effect allows us to obtain a high heating rate with uniform heating at relatively low temperature during short time of application of the constraint (typically, a few minutes). For example, a fully dense polyimide (PI) was obtained with Young's modulus of 4.4 GPa with FAST operated at 200°C and under pressure of 147 MPa [13]. Recently, optimization of FAST for PI polymer was performed [14] at higher temperature (up to 350°C) and lower pressure (40 MPa) during 5 min. Under these operating conditions, the resulting mechanical properties of the PI samples are significantly improved compared to those found in the archival literature [13].

In our present work, we take an approach based on FAST to elaborate dense PTFE polymer materials from PTFE powder. We review first the essentials of experimental apparatus and experimental conditions/protocols, and especially of FAST. Next we discuss the crystallinity degree, thermal stability, molecular structure from vibrational spectroscopy of the PTFE powder and sintered samples. Finally, we compare the stress-strain curves of sintered PTFE samples with the theory proposed by Haward and Thackray [15, 16].

II. Experimental

A. Raw material and sample fabrication

PTFE powder was purchased from Hostaflon TF 1620 (Hoechst). The determination of the size distribution is realized according to a statistical analysis of a large set of scanning electron microscopy images (an example is shown in Fig. 1(a)).

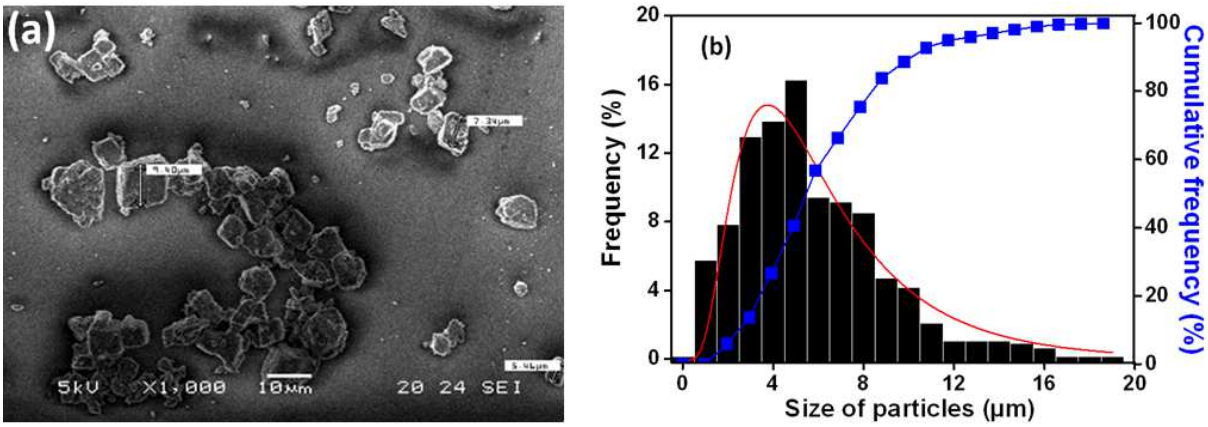

Figure 1:(a) Typical SEM micrograph of dispersed PTFE particles in 2-propanol showing roughly spherical particles, (b) diameter histogram for all data collected from different areas of dispersed PTFE particles.

PTFE powder is dispersed in 2-propanol which is stirred during five hours and deposited on a slide which is then dried under ambient atmosphere. As a result, Fig. 1(b) shows the resulting particle size histogram. A statistical analysis on different areas of the set of images (~760 measurements) shows that the size distribution follows a log-normal law $f(x) = y_0 + \frac{1}{\sigma\sqrt{2\pi}}\exp\left[-\frac{1}{2}\cdot\left(\frac{\ln(x/\mu)}{\sigma}\right)^2\right]$, where x denotes particle diameter, $\sigma = 5.44 \pm 0.61$ μm is the average value of the particle diameter, μ is the standard deviation and $y_0 (= 0.04)$ is an adjustable parameter.

The FAST experimental setup HP 25/1 (FCT GmbH, Germany) used in this investigation is shown in Fig. 2(a).

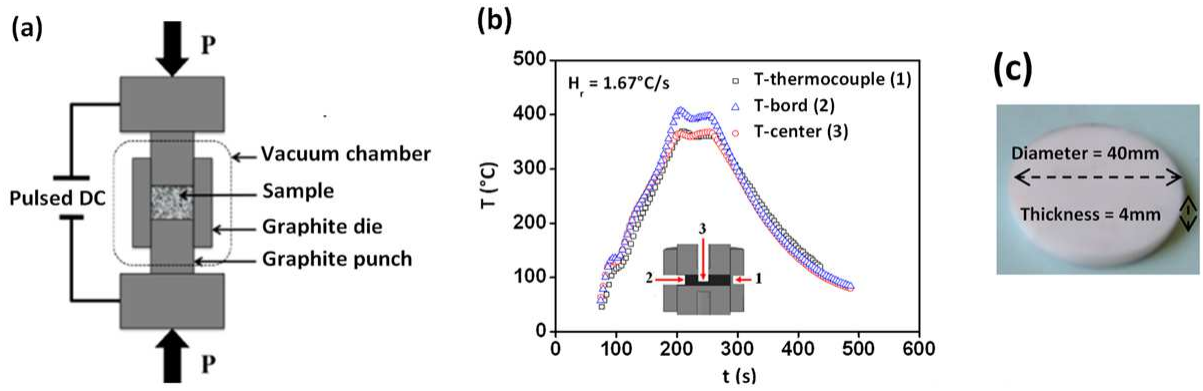

Figure 2:(a) Illustrating the FAST equipment, (b) Example of a thermal program used for FAST processing of PTFE at 380 °C and heating rate of 1.67°C/s,(c) typical discoidal samples.

The sintering mold has a cylindrical shape and is adapted to the apparatus providing the uniaxial compaction force. The 40 mm-inner diameter and 60 mm-outer diameter die is filled with 15 g of PTFE powder which is then heated to reach the prescribed temperature cycle by an automatically adjusted pulsed current generator. In order to guarantee the electrical circuit closure, all parts of the setup (die, punch, electrode, spacer) are made of graphite [17]. An electrical pulsed current (~2 kA) [18] is applied simultaneously with a compressive pressure (25 MPa) that is largely sufficient to provide an effective compaction of the PTFE particles since the yield strength of PTFE at room temperature is about ~12.5 MPa and decreases by increasing temperature [19].

To specify the sintering temperature, temperature gradients are first adjusted. An inhomogeneous temperature distribution in the sintered sample is observed and measured at two positions: center (3) and edge (2) of sintered powder as reported in Fig. 2(b). A third measurement (1) made by a thermocouple positioned at 3-4 mm from the sample side in the graphitic die is used to control the processing temperature. A slight difference is identified where a maximum difference can reach 20°C but it remains significantly smaller than the values reported in the literature [20-21]. To address this problem, the sintering temperature is fixed at 380 °C in order to keep the temperature near to the melting temperature (327°C) of PTFE. In addition, the holding time (t_s) and the heating rate H_r are respectively set to 60 s and 1.67, 2.67, or 3.33° C/s. Finally, the sintered samples have a discoidal shape with

thickness~4 mm and diameter of 40 mm (Fig. 2(c)). In what follows, the samples will be referenced as $PTFE_L$, $PTFE_I$, $PTFE_H$ where the index L (Lower heating rate=1.67 °C/min), I (Intermediate heating rate=2.67 °C/min) and H (High heating rate=3.33 °C/min), respectively.

B. Characterization

Differential Scanning Calorimetry (DSC) experiments are carried out with a PerkinElmer Series 7 DSC at heating and cooling rate of 10 °C/min within the range 30-400 °C. The calibration procedure is to run indium and zinc standards under the normal test conditions and measure the heat of fusion value and melting onset temperature. TGA is performed using a Pyris1 TGA (Perkin-Elmer, Inc., USA) instrument heated from room temperature to 700 °C at a heating rate of 20 °Cmin^{-1} under nitrogen purge. Samples of 30 mg are placed and sealed in aluminum pans. A purge gas flow rate of 40 ml/min is used. The microstructure of sintered PTFE samples is obtained by micrographs of cryo-fractured surfaces using a FEI ESEM XL30 scanning electron microscope (SEM). Typical SEM micrographs, shown in Fig. 3, sintered with T_s=380°C and H_r=1.67°C/s indicate a densely "micro-fibrils" structure.

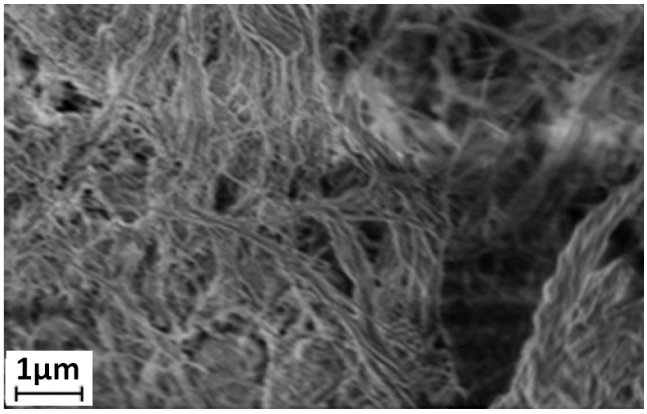

Figure 3: Typical SEM image of fractured surfaces of PTFE sample sintered with T_s=380°C and H_r=1.67°C/s. The scale bar corresponds to 1μm.

Additionally, the chemical structure the samples is characterized by Raman and Attenuated Total Reflexion Fourier Transform Infrared (ATR-IR) spectroscopies. Raman spectra of PTFE samples are recorded using a micro spectrometer (SOL, Instruments, Ltd) equipped with a (He-Ne, 632 nm) laser and a CDD sensor. ATR-IR spectroscopy is carried out on a Bruker VERTEX 70 FT-IR spectrometer. Acquisition is performed with wavenumber ranging from 4000 to 600 cm^{-1}, averaged with 20 scans at a resolution of 2 cm^{-1}. Tensile and three bending tests are performed using a machine testing Instron 3369 model at room temperature

using parallelipipedic samples with dimensions35mm × 4mm × 1.5mmwere loaded until failure at a crosshead speed of 2 mmmin^{-1}.

III. Results and discussion

A. Correlating processing conditions and microstructure

Firstly, the degree of crystallinity X_m of PTFE samples sintered under different conditions is measured by considering the DSC thermograms shown in Fig. 4.

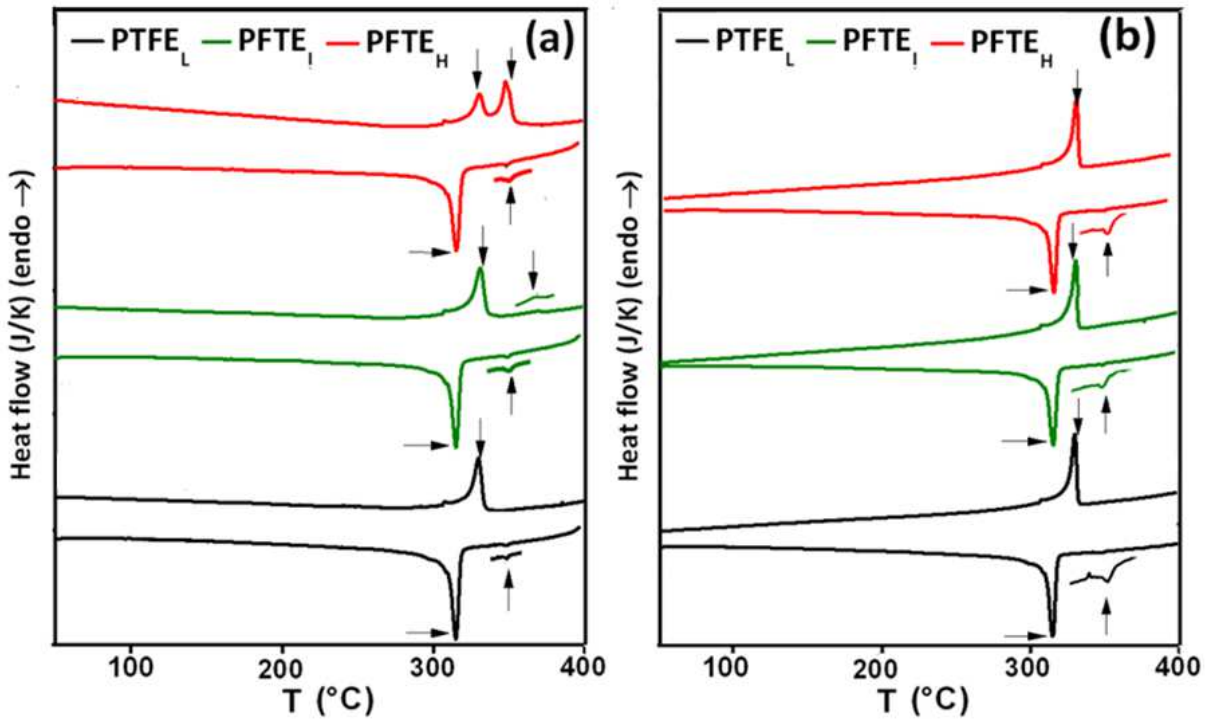

Figure 4: (a) DSC traces of the first heating and cooling cycles for 3 PTFE samples (hereafter denoted as $PTFE_L$, $PTFE_I$ and $PTFE_H$) at heating rate of 20 °Cmin^{-}1 under nitrogen atmosphere, (b) same as in (a) for the second heating and cooling cycle.

The values reported in Table 1 are obtained from the crystallization enthalpy measurement.

Table 1: Thermal transitions of $PTFE_L$, $PTFE_I$ and $PTFE_H$. Crystallinity degrees (X_m, X_c) calculated from (fusion and crystallization enthalpies, respectively) measured in the two cycles ($\Delta H^{PFTE}{}_0$= 82 J/g [23]).

Sample	1st cycle				2nd cycle			
	Melting		Crystallization		Melting		Crystallization	
	$T_m{}^{peak}$ (°C)	X_m (%)	$T_c{}^{peak}$ (°C)	X_c (%)	$T_m{}^{peak}$ (°C)	X_m (%)	$T_c{}^{peak}$ (°C)	X_c (%)
$PTFE_L$	330	17.78	314	22.14	329	18.69	314	22.70
$PTFE_I$	329	18.38	314	22.84	328	18.72	314	22.84
$PTFE_H$	330	18.67	314	22.67	329	18.57	314	23.10

For all samples two cycles (heating cycle from 30 to 400 °C followed by a cooling cycle from 400 to 30 °C) are performed. Two peaks are identified in Fig. 4(a): an endothermic peak (heating cycle) at 330 °C corresponding to the melting of the crystalline phase and another peak (cooling step) at 314 °C related to the polymer crystallization. The positions of the two peaks are practically unchanged for the subsequent second cycle as shown in Fig. 4(b). These results clearly indicate that the three samples are identical in terms of crystallinity and melting profile, suggesting that these two polymers are subjected to identical thermal history. This suggests that the microstructural changes are reversible in accordance with the results reported by Canto and coworkers [22] for PTFE samples sintered by cold compaction process. As can be seen in Fig. 4, a second weak peak of melting is also observed in the first cycle at 362 °C ($PTFE_L$) and 367 °C ($PTFE_I$, $PTFE_H$). These peaks can be associated to the melting of the extended chain crystals [23]. It is also worth noting that a second weak peak is also detected in both 1st and 2nd crystallizations at typically 347°C for all samples.

Polymer crystallinity can be determined with DSC by quantifying the heat (ΔH_f) associated with fusion of the polymer. This heat is reported as percent crystallinity by normalizing the observed heat of fusion to that of a 100 % crystalline sample of the same polymer (ΔH_f^0=82 J/g) [23]. The results for the three samples studied are summarized in Table 1: X_m is found to decrease slightly when the heating rate is increased. We further note that the value of X_m of as-received PTFE powder (~60%) is much larger than the corresponding values of the sintered PTFE samples in agreement with many observations in the archival literature [6, 22, 23].

The curves of weight change percentage as function of temperature and their derivatives are shown in Fig. 5.

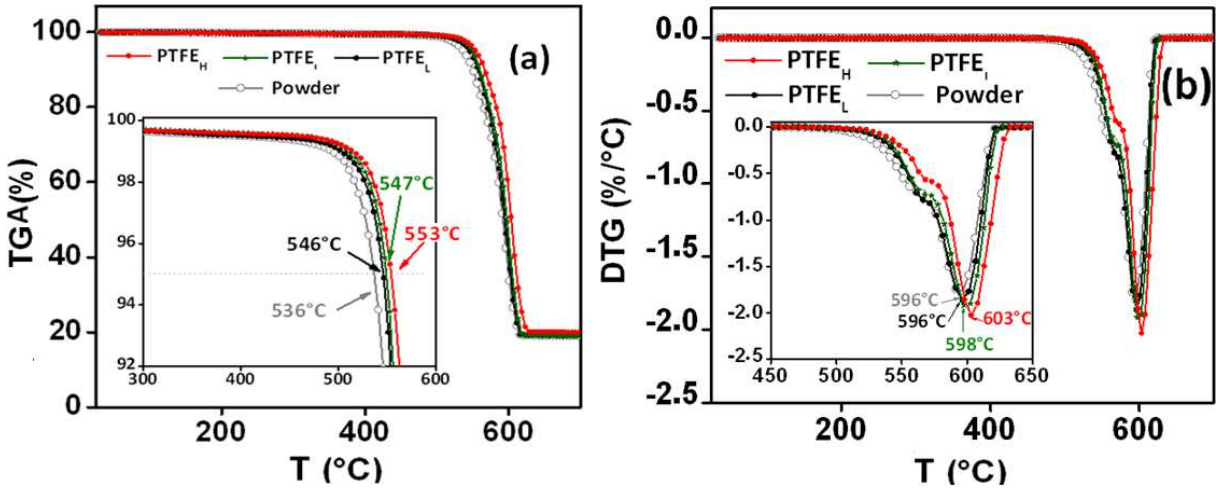

Figure 5: (a) TGA thermal curves (weight percentage versus temperature) of $PTFE_L$, $PTFE_I$ and $PTFE_H$ at heating rate of 20 °Cmin^{-}1 under nitrogen atmosphere; for comparison, the case of PTFE powder is shown, (b) same as in (a) for the derivative weight percentage (DTG) versus temperature.

The three samples exhibit similar stable thermal behaviors until~500°C. Weight loss is apparent between ~500°C and temperature degradations T5 (loss of 5 wt.%) which are 536±1 °C for the pristine PTFE powder, 546±1 °C, 547±1 °C and 553°C±1 °C for PTFE1, PTFE2 and PTFE3, respectively (Fig. 5(a)). The corresponding temperatures of maximal degradation are close to 596±1 °C, 596±1 °C, 598±1 °C and 603±1 °C (Fig. 5(b)), respectively. The larger heating rate employed during FAST, the more important thermal stability is obtained without weight loss.

To identify the chemical structure changes of PTFE fabricated by FAST with varied heating rates, both Raman and ATR-IR spectroscopies are used (Fig. 6).

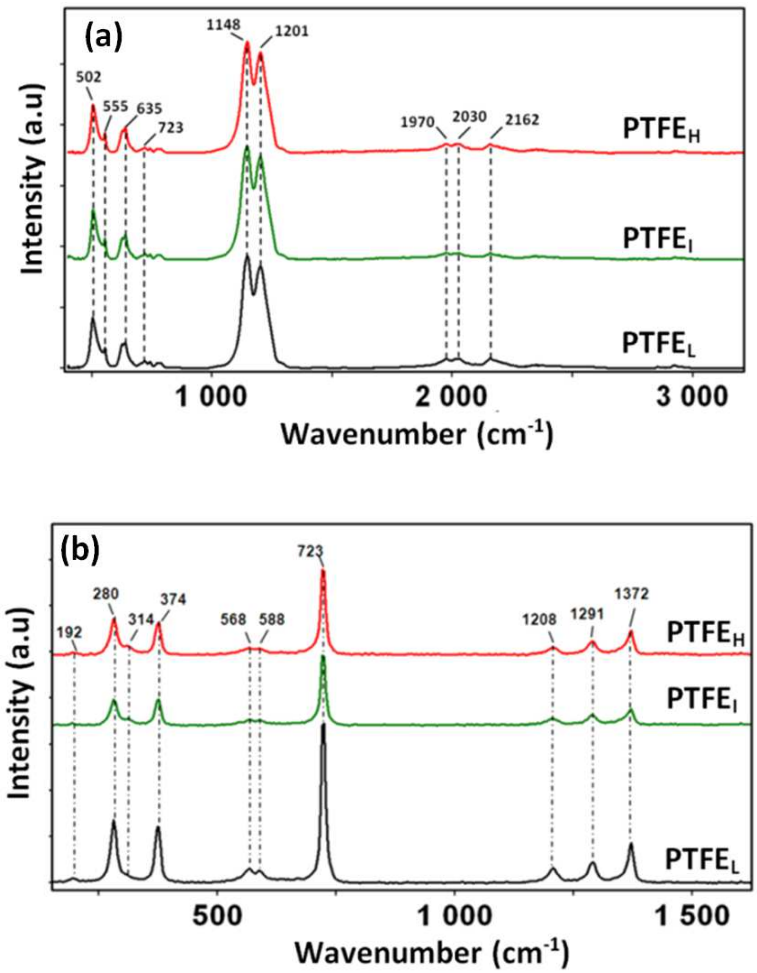

Figure 6: Infrared (upper) and Raman (lower) spectra of PTFE samples synthesized by FAST with three values of heating rate.

Comparing the well-known Raman and IR spectra of PTFE reported in the literature [24] and our measurements (Fig. 6(a)), we observe the CF_2 stretching vibrations in the IR bands at 1148 and 1202 cm^{-1}. Other dominant bands are observed at 502, 555, 635 and 723 cm^{-1} which are respectively assigned to the CF_2 twisting, CF_2 bending, CF deformation and CF_2 scissoring. Complementary information can be deduced from the Raman spectrum illustrated in Fig. 6(b). The CF_2 rocking, wagging, twisting, symmetric and asymmetric stretching modes are characterized by 192, 280, 374, 723, and 1291 cm^{-1} bands, respectively. Other dominant bands are observed at 502, 555, 635 and 723 cm^{-1} which are respectively assigned to the CF_2 twisting, CF_2 bending, CF deformation and CF_2 scissoring. In addition, very weak peaks located around 2000 (1970, 2030 and 2192) cm^{-1} and 2900 cm^{-1} can be also seen in Fig. 6(a). These peaks are characteristic of electrically conductive species originating probably from the graphite used to guarantee the electric contact between the powder and current source [25-28].

In addition, Raman spectroscopy is found to be more sensitive to highly polarizable groups such as C-C bands characterized by 1208 cm^{-1} band (Fig. 6(b)). It is also worthy to note that the strong Raman bands at 723 cm^{-1}corresponds to a very weak IR band. Raman and IR spectroscopies can be used to distinguish crystalline from amorphous phases of polymer materials [29-32]. The CF stretching observed at 635 cm^{-1} IR band and 1379 cm^{-1} Raman band is assigned to the crystalline zone of PTFE [32]. This is dictated by the symmetry of the vibrational mode of the crystal space group [30]. Moynihan [33] suggested that the amorphous state can be detected from the 700-800 cm^{-1} IR bands and found that the IR-peak intensity of amorphous bands decreases with an increase of crystallinity in PTFE. The most salient point is that no spectral features are detectable for the three sintered PTFE samples processed with different heating rates.

B. Mechanical properties

Several methods are used to characterize the mechanical behavior in tensile tests performed under different strain rates using samples fabricated with different heating rate process parameters. From these methods, the Young's modulus, yield stress, tensile strength, and the elongation at break can be obtained. Figure 7(a) compares the dependence of the true stress-strain curves deduced from three bending tests.

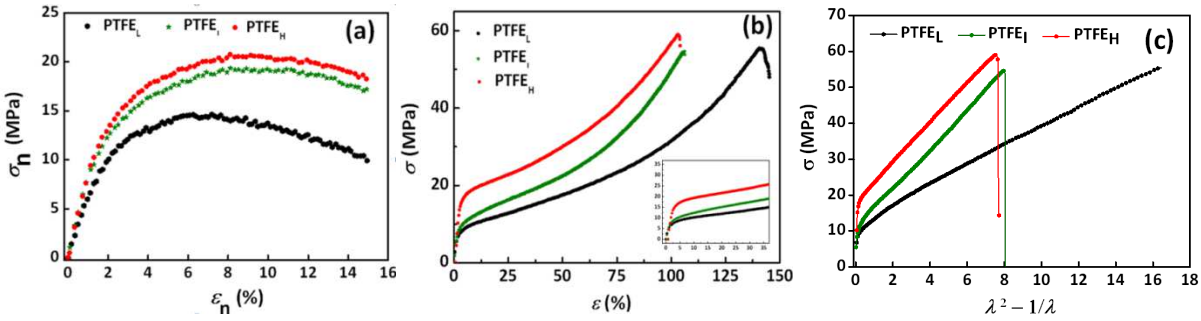

Figure 7: Mechanical behavior of PTFE samples sintered at T_s=380°C and different heating rate values: (a) stress-strain bending curves, (b) tensile properties, and (c) fit of the experimental data from the stress-strain tensile curves to the Gaussian equation.

The stress-strain curves shown in Fig. 7(a) are typical of the plastic character of our samples. It is possible to quantify the brittleness behavior in both ductile and brittle polymer materials

by using additional mechanical tests coupled to appropriate models [34]. For instance, on the basis of this approach, Brostow [35] determined the brittleness index value of a ductile PTFE (0.375 % Pa 10^{-10}) that is very lower compared to brittle polymers such as PS (8.783 % Pa 10^{-10}). The values of the flexural strength of PTFE samples, obtained at the maximum of stress of each curve of Fig. 7(a), are respectively 14.62 ($PTFE_L$), 19.34 ($PTFE_I$) and 20.75 MPa ($PTFE_H$). This result shows a direct heating rate parameter dependence of the flexural strength that can be related to the inhomogeneous temperature distribution in the sintered samples (Fig. 2). Because similar trend is also seen in tensile curves (Fig. 7(b)), other microstructural aspects can impact the heating rate versus mechanical behavior dependence, e.g. entanglement density (see Table 2). More thought is needed to check the impact of other factors such as fibril formation, size and distribution of crystalline domains. [36]. Our samples show no brittleness behavior which is consistent with their very small void fraction. It is also worth noting that increasing the heating rate generally enhances the sintering process by increasing the flexural strength associated to the increase of elongation magnitude.

We turn now to assess how the sintering temperature and heating rate affect the mechanical properties in tensile mode until failure. Figure 7(b) depicts the true stress-strain curves conducted at a fixed strain rate and room temperature. With constant volume, the true stress-strain σ vs ϵ and nominal stress-strain σ_n vs ϵ_n representations are defined as $\sigma = \sigma_n(1+\varepsilon_n)$ and $\varepsilon = ln(1+\varepsilon_n)$ with the hypothesis of a constant volume in tensile. The extension ratio $\lambda = 1+\varepsilon$ is defined as the extended length over the original length. We observe that all samples show a good ductility with an extension ratio ranging from 300 to 400 % and a good tensile strength when the sintering temperature is closed to 380°C. At this sintering temperature, increasing the heating rate leads to a significant loss of ductility with a slight increase in stress strength from 54 to 58 MPa. Additionally, significant energy dissipation occurs when PTFE samples are uniaxially stretched thanks to the development of a fibrillation structure that is visible in SEM micrographs (Fig. 3) [37-38].

It is also worth noting that a good correlation is found between thermal stability and tensile properties when the heating rate is changed. Indeed, the mechanical behavior is generally enhanced when the heating rate is increased. The mechanical characteristics shown here are in agreement with those published in the archival literature for PTFE samples fabricated by conventional methods [6,7,15,16,39]. In order to understand the mechanical behavior observed in sintered PTFE samples under tensile test, the theory proposed by Haward and Thackray (HT) is used [15-16]. This model attempts to describe the large stress-strain curves observed in semi-crystalline thermoplastics. Using HT theory, the experimental results can be

interpreted by means of a spring and dashpot model in which the spring defines a strain hardening process according to the theories of high elasticity. Under uniaxial stretching, the plastic deformation is represented by the Gaussian equation $\sigma = Y_0 + G_P\left(\lambda^2 - \frac{1}{\lambda}\right)$, where Y_0 is the extrapolated yield stress representing the frictional forces during deformation and G_P is a strain-hardening modulus corresponding to the plastic deformation in semi-crystalline polymers. From the results shown in Fig. 7(c), good agreement can be seen between the actual stress-strain of sintered samples and the Gaussian equation (Fig.7(c)). Values for the constants Y_0 and G_P are shown in Table 2: Y_0 is found be in the range 10.94-18.05 MPa [16].

Table 2: Strain hardening modulus and extrapolated yield stress of FAST-PTFE samples according to the Gaussian equation (data plotted in Fig. 7). Room temperature.

Sample	Heating rate H_r (°C/s)	Y_0 (MPa)	G_p (MPa)	M_e (g/mol)
$PTFE_L$	1.67	11.62	2.75	2035
$PTFE_I$	2.67	10.94	5.45	1013
$PTFE_H$	3.33	18.05	5.55	1011

Knowledge of the strain-hardening modulus G_P can inform us about the network properties of sintering PTFE especially on the role of the entangled chains in the deformation process. Values G_P are determined by fitting the linear response after the onset of yielding of each curve of the sintered samples (Fig.7(c)) and are found to be in the range 2.75-5.55 MPa (Table 2) indicating a change in corresponding entanglement molecular weight M_e according to the conventional theory of rubber elasticity: $G_P = \frac{\rho RT}{M_e}$. It is worth noting that, for samples sintered with 1.67 and 2.66°Cs^{-1}, $G_P = 5.45$ and 5.55 MPa, respectively. Consequently, the entanglement density is expected to be significantly reduced and plays a significant role in the deformation mechanisms. The high value of G_P obtained by fitting the experimental curves to the Gaussian equation are close to that observed by Haward for PTFE polymer, i.e. G_P =5.0 MPa [16].

IV. Concluding remarks

By adopting an appropriate choice of process parameters, a series of dense PTFE samples is obtained. The basic level of microstructure characterization is achieved by Raman and IR vibrational techniques in order to identify the chemical structure of the sintered PTFE samples fabricated by FAST. The crystallinity and thermal stability are also reported and discussed. The results given in this paper reinforce the conclusion from earlier work that heating rate during FAST affects significantly the bending and tensile properties. Furthermore, the series of true stress-strain curves for PTFE fit in with the Gaussian equation proposed by HT. We close by noting that the ability of FAST to densify rapidly polymeric materials having high viscosity is the primary advantage of this technique. By controlling the processing parameters one can tailor the mechanical response for specific end uses. The interesting mechanical properties of PTFE samples make the application of FAST a potential way to improve its quality in a cost-effective manner.

Acknowledgments

The authors and especially A.M. are gratefully acknowledging INSA Lyon, France for providing partial funding of this work.

References

[1] L.A. Wall, *Technology of Fluoropolymers*, L.A. Wall (Ed.), 2ed edn. Wiley-Interscience, New York, 1972, https://doi.org/10.1002/pol.1972.110100418.

[2] J.C. Salamone, Polymeric Materials, Encyclopedia vol.4. CRC Press, Boca Raton 1996, ISBN 0-8493-2470-X.

[3] H. Teng, Overview of the development of the fluoropolymer industry, Appl. Sci. 2 (2012) 496-512, doi: 10.3390/app2020496.

[4] C. A. Sperati and H. W. Starkweather, Fluorine-containing polymers. II. Polytetrafluoroethylene, Fortschritte Der Hochpolymeren-Forschung 2 (1961) 465–495, https://doi.org/10.1007/BFb0050504.

[5] Q. Sheng, Tribological and mechanical characterization of thin polymer films. Dissertation Northeastern University Boston, Massachusetts, US. 2013, http://hdl.handle.net/2047/d20004893.

[6] P. J. Rae and D. M. Dattelbaum, The properties of polytetrafluoroethylene in compression, Polymer 45 (2004) 7615–7625, https://doi.org/10.1016/j.polymer.2004.08.064.

[7] P. J. Rae and E. N. Brown, The properties of polyfuoroethylene in tension, Polymer 46 (2005) 8128-8140, https://doi 10.1016/j.polymer.2005.06.120.

[8] S. Hambir and J. P. Jog, Sintering of ultra-high molecular weight polyethylene, Bull. Mater. Sci. 23(3) (2000) 221–226, https://doi.org/10.1007/BF02719914.

[9] K. Al Jebawi, B. Sixou, R. Séguéla, G. Vigier, and C. Chervin, Hot compaction of polyoxymethylene, part 1: Processing and mechanical evaluation, J. Appl. Polym. Sci. 102 (2006) 1274-1284, https://doi.org/10.1002/app.24342.

[10] D. Jauffrès, O. Lame, G. Vigier, and F. Doré, Microstructural origin of physical and mechanical properties of ultra-high molecular weight polyethylene processed by high velocity compaction, Polymer 48 (2007) 6374-6383, https://doi.org/10.1016/j.polymer.2007.07.058.

[11] B. Poitou, F. Dore, and R. Champomier, Mechanical and physical characterizations of polytetrafluoroethylene by high velocity compaction, Int. J. Mater. 1 (2009) 657-660, https://doi.org/10.1007/s12289-009-0649-8.

[12] P. Cavalier, *Spark Plasma Sintering of Materials: Advances in Processing and Applications*. Springer, Switzerland 2019, ISBN: 978-3-030-05327-7.

[13] M. Omori, A. Okubo, K. Gilhwan, and Y. Hirai, Consolidation of thermosetting polyimide by the spark plasma system, J. Mater. Synth. Proc. 5 (1997) 1236–1279.

[14] M. Schwertz, P. Ranque, S. Lemonnier, E. Barraud, A. Carrado, M.F. Vallat, and M. Nardin, Optimization of the spark plasma sintering processing parameters affecting the properties of polyimide, J. Appl. Polym. Sci. 132 (2015) 41542-41552, https://doi.org/10.1002/app.40783.

[15] G. Thackray and R.N. Haward, The use of a mathematical model to describe isothermal stress-strain curves in glassy thermoplastics, Proc. R. Soc. London A302 (1968) 453-472.

[16] R.N. Haward, Strain hardening of thermoplastics, Macromolecules 26 (1993) 5860-5869, https://doi.org/10.1021/ma00074a006,

[17] R. Orru, R. Licheri, A.M. Locci, A. Cincotti, and G. Cao, Consolidation/synthesis of materials by electric current activated/assisted sintering, Mater. Sci. Engng. R 63 (2009) 127-287, doi: 10.1016/j.mser.2008.09.003.

[18] A. Munir, U. Anselmi-Tamburini, and M. Ohyanagi, The effect of electric field and pressure on the synthesis and consolidation of materials: A review of the spark plasma sintering method, J. Mater. Sci. 41(2006) 763-777, https://doi.org/10.1007/s10853-006-6555-2.

[19] S. Ebnesajjad and P.R. Khaladkar, *Fluoropolymers Applications in Chemical Processing Industries*. William Andrew Inc., New York, 2017, eBook ISBN**:** 9780323461153.

[20] J. Räthel, M. Herrmann, and W. Beckert, Temperature distribution for electrically conductive and non-conductive materials during Field Assisted Sintering (FAST), J Eur. Ceram**.** Soc. 29 (2009) 1419–1425, doi 10.1016/j.jeurceramsoc.2008.09.015.

[21] M. Jaafar, Elaboration et caractérisation des nano-composites alumine-Sic, Dissertation, INSA, Lyon France, 2011.

[22] R.B. Canto, N. Schmitt, J. Carvalho, and R. Billardon, Experimental identification of the deformation mechanisms during sintering of cold compacted polytetrafluoroethylene (PTFE) powders, Polym. Eng. Sci. 55 (2011) 2220-2235, https://doi.org/10.1002/pen.21994.

[23] Y.P. Khana, The melting temperature of polytetrafluoroethylene, J. Mat. Sci. Lett. 7 (1988) 817-818, https://doi.org/10.1007/BF00723770.

[24] J. Mihály, S. Sterkel, H.M. Ortner, L. Kocsis, L. Hajba, É. Furdyga, and J. Minka, FTIR and FT-Raman spectroscopic study on polymer based high pressure digestion vessels, Croat. Chem. Acta. 79(3) (2006) 497-501.

[25] D.D Fazullin, G.V. Mavrin, M.P. Sokolov, and I.G. Shaikhiev, Infrared spectroscopic studies of the PTFE and Nylon membranes modified polyaniline, Mod. Appl. Sci. 9(1) (2015), doi:10.5539/mas.v9n1p242.

[26] Y. Zhang, X. Cheng, X. Jiang, J. J. Urban, C.H. Lau, S. Liu, and L. Shao, Robust natural nanocomposites realizing unprecedented ultrafast precise molecular separations. Mater. Today. 36 (2020) 40-47, doi: 10.1016/j.mattod.2020.02.002

[27] Y. Zhang, J. Ma, and L. Shao, Ultra-thin Trinity Coating Enabled by Competitive Reactions for Unparalleled Molecular Separations, J. Mater. Chem. A 8 (2020) 5078-5085, doi: 10.1039/C9TA12670H.

[28] Y. Lan, P. Peng, and P. Chen, Preparation of polymers of intrinsic microporosity composite membranes incorporated with modified nano-fumed silica for butanol separation, Adv. Polym. Technol. 37(8) (2018) 3297-3304, doi.org/10.1002/adv.22114.

[29] C.M. Snively, J.L. Koenig, IR and Raman Spectroscopies, *Polymer Applications. Encyclopedia of Spectroscopy and Spectrometry*, Third edition, (2017) 365-371. See also J.L. Koenig, *Spectroscopy of Polymers*; American Chemical Society: Washington, DC 1992. https://doi.org/10.1002/ange.19931050650

[30] W.G. Fateley, F.R. Dollish, N.T. McDevitt, and F.F. Bentley, Infrared and Raman Selection Rules for Molecular and Lattice Vibrations: The Correlation Method. Wiley, New York, 1972, doi:10.1016/0022-2860(73)85205-6.

[31] P. Musto, S. Tavone, G. Guerra, and C. De- Rosa, Evaluation by Fourier transform infrared spectroscopy of the different forms of syndiotactic polystyrene samples, J. Polym. Sci. Pol. Phys. 35 (1997) 1055–1066, https://doi.org/10.1002/(SICI)1099-0488(199705)35:7<1055::AID-POLB5>3.0.CO;2-V.

[32] G. Legeay, A. Coudreuse, J.M. Legeais, L. Werner, A. Bulou, J.Y. Buzare, J. Emery, and G. Silly, AF fluoropolymer for optical use: spectroscopic and surface energy studies; comparison with other fluoropolymers, Eur. Polym. J. 34 (1998) 1457–1465, https://doi.org/10.1016/S0014-3057(97)00289-9.

[33] R.E. Moynihan, The molecular structure of per fluorocarbon polymers, Infrared studies on polytetrafluoroethylene, J. Am. Chem. Soc. 81(1959) 1045–1050, https://doi.org/10.1021/ja01514a009

[34] I. El Aboudi, A. Mdarhri, C. Brosseau, A. Montagne, F. Elhaouzi, Z. Bouyahia, and A. Iost, Investigating carbon-black-filled polymer composites' brittleness, Polym. Bull. (2019) 1-11 doi:10.1007/s00289-019-03000-w

[35] W. Brostow and H.E. Hagg Lobland. Brittleness of materials: Implications for composites and a relation to impact strength, J. Mater. Sci. 45 (2010) 242–250, doi 10.1007/s10853-009-3926-5

[36] I. Elaboudi, A. Mdarhri, C. Brosseau, A. Nourdine, M. Rzaizi, and L. Servant, Comparing the sorption kinetics of poly-tetrafluoroethylene processed either by extrusion or spark plasma sintering. **190** (2020) 122192, doi: 10.1016/j.polymer.2020.122192

[37] S. Bandyopadhyay, R. Kamalakaran, S. Gupta, R. Mazumdar, B. Sathapathy, and AK. Ghosh, Fibrillation of teflon in polymer matrix, in Proceedings of the International Conference on Advances in Polymer Technology (APT'10), Kochi, India, February (2010) 71–74.

[38] B. Patham and M.P. Poornendu Thejaswin, A preliminary investigation of ductility-enhancement mechanism through in situ nanofibrillation in thermoplastic matrix composites, J. Polym. (2013) 1-9, doi.org/10.1155/2013/424015

[39] N. Brown and M.F. Parrish, Effect of liquid nitrogen on the tensile strength of polyethylene and polytetrafluroethylene, Polym. Lett. Edit. 10 (1972) 777-779, https://doi.org/10.1002/pol.1972.110101004

[40] L.R.G. Treloar, The Physics of Rubber Elasticity, 3rd Edn, Clarendon Press, Oxford, 1975, https://doi.org/10.1002/pi.4980080107

Graphical Abstract

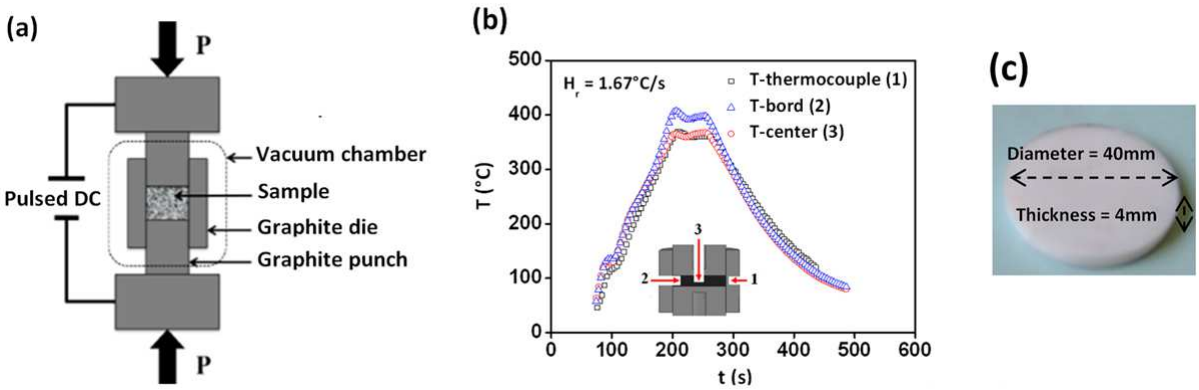

Illustrating the FAST equipment, (b) Example of a thermal program used for FAST processing of PTFE at 380 °C and heating rate of 1.67°C/s, (c) typical discoidal samples.